Available online at www.sciencedirect.com

SciVerse ScienceDirect

Procedia Engineering 00 (2015) 000–000

Procedia Engineering

www.elsevier.com/locate/procedia

The 13th Hypervelocity Impact Symposium

MMOD puncture resistance of EVA suits with shear thickening fluid (STF) – Armor™ absorber layers

Colin D. Cwalina[a], Richard D. Dombrowski[a], Charles J. McCutcheon[a], Eric L. Christiansen[b], and Norman J. Wagner[a]*

[a]*Department of Chemical and Biomolecular Engineering, University of Delaware, Newark, DE 19716*
[b]*NASA Johnson Space Center, Houston, TX 77058*

Abstract

Absorber layers comprised of shear thickening fluid (STF) intercalated Kevlar® (STF-Armor™) are integrated within the standard extra-vehicular activity (EVA) suit and tested for efficacy against both needle puncture and hypervelocity impact (HVI) tests characteristic of micrometeoroids and orbital debris (MMOD). An improvement in puncture resistance against hypodermic needle threats is achieved by substituting STF-Armor™ in place of neoprene-coated nylon as the absorber layer in the standard EVA suit. The prototype lay-ups containing STF-Armor™ have the benefit of being 17% thinner and 13% lighter than the standard EVA suit and the ballistic limit is identified in HVI testing. The results here demonstrate that EVA suit lay-ups containing STF-Armor™ as absorber layers offer meaningful resistance to MMOD threats.

Keywords: Shear thickening fluids; micrometeoroids and orbital debris; extra-vehicular activity suit; hypodermic needle

1. Introduction

In low-earth orbit, astronauts performing extra-vehicular activities (EVA) are exposed to the direct threat of micrometeoroid and orbital debris (MMOD) as well as cut and puncture hazards when coming into contact with materials damaged by MMOD. Micrometeoroids are natural particles originating from comets and asteroids while manmade orbital debris consists largely of aluminum based compounds from spacecraft and satellite debris. Micrometeoroid velocities vary widely across the solar system from 11-72 km/s while orbital debris particles in low-earth orbit travel from 1-15 km/s with an average velocity of 9 km/s. These highly energetic MMOD particles are a serious threat to spacecraft as well as EVA missions. As the desired level of MMOD protection increases, the shield weight required typically increases exponentially [1]. Such increases in shielding weight and reduction in flexibility are undesirable for astronauts, hence the motivation for the work presented here that explores the possible benefits of replacing existing absorber layers with flexible, lightweight nanocomposites comprised of correctional Kevlar® woven fabric intercalated with energy absorbing shear thickening fluids.

* Corresponding author. Tel.: +1-302-831-8079; fax: +1-302-831-1048.
E-mail address: wagnernj@udel.edu.

1.1. EVA Suit

The design of the current extra-vehicular activity (EVA) suit (Figure 3) derives from the classic Whipple Shield concept [2] used for vehicle shielding. Our test material lay-ups are based on the design of a standard EVA lay-up reported by ILC Dover [3]. The outer Orthofabric layer serves as a sacrificial bumper layer where incoming hypervelocity particles are shocked into a high energy state with the aim of fragmenting, melting, or in the best case scenario, vaporizing the projectile. This Orthofabric layer is followed by several layers of aluminized Mylar. The Mylar is a radiation shield, but serves as a spacer layer for distributing the momentum of the projectile's debris cloud over a larger area before reaching the absorber layers. In the standard EVA suit, two layers of neoprene-coated nylon are used to absorb the debris cloud before it can reach the urethane-coated bladder cloth lining the pressurized air bladder.

1.2. Shear Thickening Fluids (STFs)

Colloidal dispersions exhibit a shear rate-dependent flow behavior reflective of the particle microstructure [4-6] as demonstrated in Figure 1. At equilibrium, the particles are distributed uniformly in the fluid due to the randomizing effect of Brownian motion and will flow with a relatively high viscosity. At low to moderate shear rates, the convective rate becomes comparable to the rate of Brownian motion and the particles adopt a new microstructure in the imposed shear flow and as a result the viscosity decreases (shear thinning). However, at higher shear rates, neighboring particles are driven into close proximity where a thin fluid layer is squeezed out from between particle surfaces and a large lubrication stress results in the formation of transient stress bearing hydroclusters [5]. The formation of hydroclusters is concomitant with an increase in the dispersion viscosity [7-9]. For concentrated colloidal dispersions, this increase in viscosity can be abrupt and violent, resulting in a rigid, solid-like response from the dispersion [10, 11]. This shear thickening phenomenon is entirely reversible in the sense that the dispersion will return to its low viscosity fluid-like state upon the removal of the shear stress.

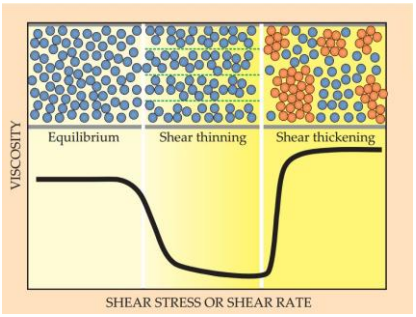

Fig 1. Flow behavior of hard-sphere colloidal dispersions (used with permission from [4]). Dispersions can exhibit either a liquid-like or solid-like response depending upon the magnitude of the applied shear stress.

1.3. STF-Armor™

The reversible fluid-to-solid transition of these dispersions has made them attractive for soft body armor applications, particularly when they are intercalated into the space between fibrils of a protective textile as STF-Armor™ [12, 13] shown in Figure 2. The textile surfaces remain dry to the touch as the STF is held between fibrils by capillary forces. Under the stresses associated with routine body movements, the dispersion shear thins and exhibits a liquid-like response that does not restrict movement. Upon an impact event that exceeds the critical stress for shear thickening, the dispersion exhibits a rigid solid-like response restricting the motion of yarns around the impact site and preventing pullout from the fabric. Protective fabrics intercalated with STF have been shown to dramatically improve the resistance to ballistic projectiles [12, 14] and puncture threats [13, 15]. MMOD particles are both a puncture and ballistic threat and thus, STF-Armor™ is an attractive technology to improve MMOD resistance without compromising weight or flexibility. The current work undertakes the first experimental investigation to establish the ballistic limit curve and needle puncture resistance of an EVA suit lay-up containing STF-Armor™ technology.

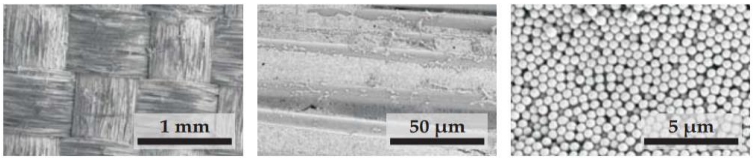

Fig. 2. A colloidal STF intercalated between fibrils of woven Kevlar® as STF-Armor™ (used with permission from [4])

2. Experimental

2.1. Materials

Figure 3 shows a schematic of the standard EVA suit lay-up along with the prototype lay-up containing STF-Armor™. The standard EVA lay-up employs two layers of neoprene-coated nylon to absorb the debris cloud [3]. In the prototype lay-ups investigated in the present work, the two absorber layers used were a commercially available STF-treated correctional Kevlar® style 1148 (300 denier, 59 x 59 yarns per inch) from Barrday (Cambridge, Ontario, Canada). Accordingly, the prototype lay-ups investigated in this study were 17 % thinner than the standard EVA lay-up and had a 13% reduction in areal density**.

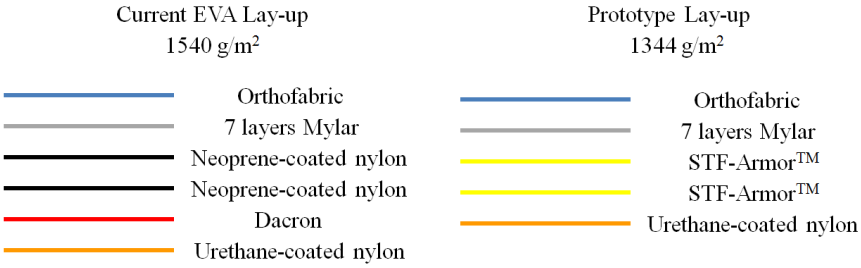

Standard EVA Lay-up

Layer	Thickness (mm)	Areal Density (g/cm²)
Orthofabric	0.56	0.049
7 layers Mylar	0.42	0.022
Neoprene-coated nylon	0.43	0.028
Neoprene-coated nylon	0.43	0.028
Urethane-coated nylon	0.32	0.027
Total	**2.16**	**0.154**

Prototype Lay-up

Layer	Thickness (mm)	Areal Density (g/cm²)
Orthofabric	0.56	0.049
7 layers Mylar	0.42	0.022
STF-Armor™	0.25	0.018
STF-Armor™	0.25	0.018
Urethane-coated nylon	0.32	0.027
Total	**1.80**	**0.134**

Fig. 3. Schematic of standard EVA lay-up (left) along with the prototype lay-up containing STF-Armor™ (right) studied in the present work along with the thickness and areal density of each layer.

2.2. Quasi-static Hypodermic Needle Puncture Testing

Hypodermic needles are complex threats. In addition to being a puncture threat from the conical tip, they also possess a continuous cutting edge. Hypodermic needles are thus ideal choices to simulate the cutting and puncture threat associated with MMOD particles [16]. Previous work shows that some aspects of material performance and damage modes at higher impact loading rates can be inferred from quasi-static testing results [17-20]. The quasi-static needle puncture testing was performed using a modified ASTM F-1342 standard with a hypodermic needle held in a chuck replacing the puncture probe as seen in Figure 4. Lay-ups containing neoprene-coated nylon, neat Kevlar®, and STF-Armor™ as absorber layers were loaded at a rate of 254 mm/min by an 18 gauge (1.270 mm barrel diameter) BD (Becton, Dickinson, and Company) PrecisionGlide™ hypodermic needle (Franklin Lakes, NJ). These needles possess a continuous cutting surface that can facilitate penetration. Force measurements were made on an Instron 5965 using a 500 N load cell.

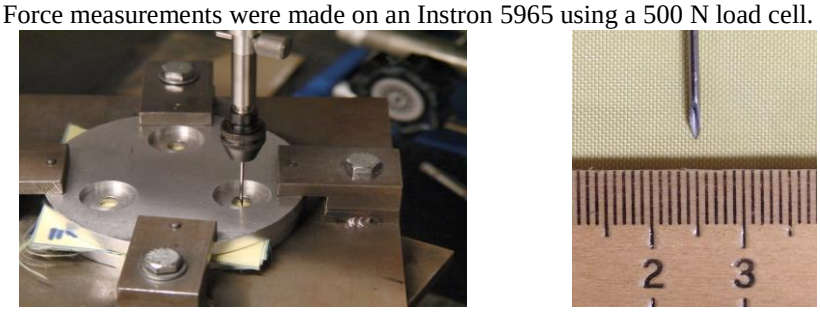

Fig. 4. Apparatus used for quasi-static puncture testing along with a close up of the 18 gauge hypodermic needle threat

**The standard EVA suit also uses a layer of Dacron polyester restraint. This Dacron layer was not included as it located behind the absorber layers.

2.3. Hypervelocity Impact (HVI) Testing

HVI testing was conducted following the protocols previously reported [21]. Test article were nominally 4" x 4" in dimension and held between two aluminum target frames with shims as shown in Figure 5. The samples were laser cut, including the holes required for mounting. The shims insure the integrity of the materials throughout the testing process by trapping the material between the plates without compressing it. The plates were secured by all tread rods, nuts, and washers. A 1 mm thick aluminum witness plate was set at a 3" standoff behind the target plate to record any debris signature.

Fig. 5. Front (left) and side (right) view of test frame articles used in this study.

Hypervelocity impact (HVI) testing was performed on the .17 caliber light gas gun at NASA's White Sands Remote Hypervelocity Test Facility. Spherical aluminum 2017-T4 (2.796 g/cm^3) projectiles were used in all tests. An ultra-high speed camera was used to observe projectile integrity immediately before impacting the target. Targets were impacted at 0º normal to the front surface in a nitrogen chamber environment kept below 1 torr. Impact velocities ranged from 4.36 – 7.40 km/s. The methods used to calculate impact velocities and the uncertainties associated with those calculations are reported in the Appendix.

3. Results and Discussion

3.1 Quasi-static Hypodermic Needle Puncture

The force experienced by the hypodermic needle was recorded as it displaced through the EVA lay-up. Twelve replicates were obtained for lay-ups with a different absorber layer: neoprene-coated nylon, neat Kevlar®, and STF-Armor™. The result of each individual replicate as well as the displacement-averaged load for each type of lay-up is reported in Figure 6.

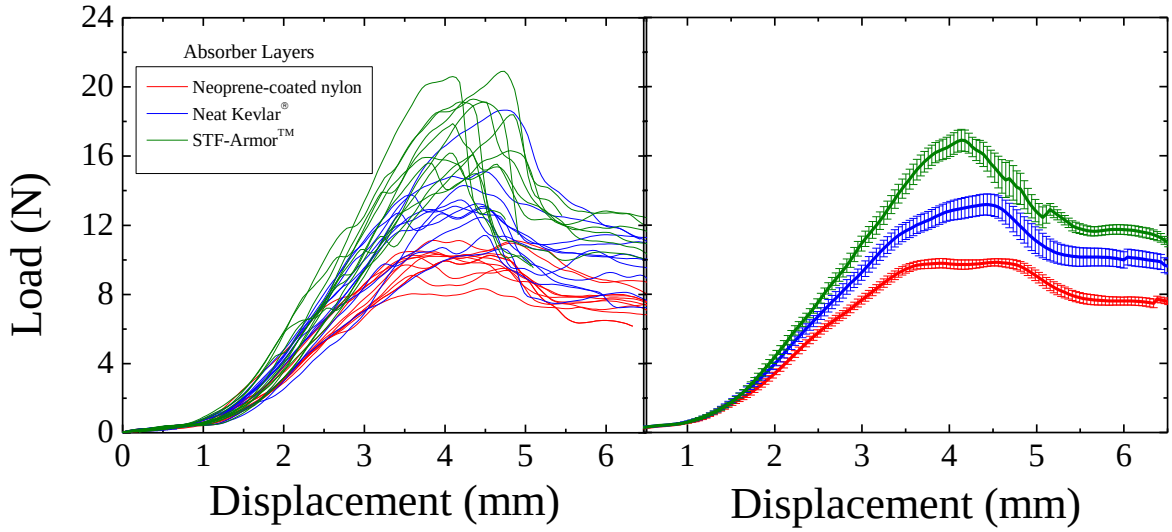

Fig. 6. (Left) Load vs. displacement curves for quasi-static hypodermic needle puncture of EVA suit containing neoprene-coated nylon (red), neat Kevlar® (blue), and STF-Armor™ (green) as absorber layers. (Right) Average load as a function of needle displacement. Error bars reflect standard error about the mean value for a given displacement.

A 35% increase in peak load is achieved by substituting neat Kevlar® (13.2 ± 0.6 N) for neoprene-coated nylon (9.8 ± 0.2 N) as the absorber layer. Substituting STF-Armor™ (16.9 ± 0.2 N) for neoprene-coated nylon results in a 72% increase in peak force resistance to needle puncture. The additional energy dissipation achieved from STF intercalation of the Kevlar® was studied in depth by Houghton *et al*. [15]. In addition to viscous dissipation occurring within the STF, the transition to the shear-thickened state couples the motion of neighboring fibers around the impact site and helps to distribution the load from the needle away from the primary fibers at the impact site. These quasi-static results suggest that replacing the neoprene-coated nylon with STF-Armor™ as the absorber layer may offer a meaningful improvement in protection against puncture threats in EVA suits.

3.2. Ballistic Limit of EVA Suit Lay-up Containing STF-Kevlar®

The ballistic limit of the prototype lay-ups containing STF-Armor™ as absorber layers is shown in Figure 7. With a limited number of experimental tests, the ballistic limit is defined as follows. The lay-up is considered to be penetrated if there is a hole in the urethane coating of the bladder cloth exceeding 1 mm and not penetrated if the urethane coating remains completely intact. If a pin-hole size puncture is observed in the urethane coating under microscopy (<< 1 mm) then that particular projectile size and velocity are considered to lie on the ballistic limit of the prototype lay-up. The full experimental test matrix is reported in Table 1.

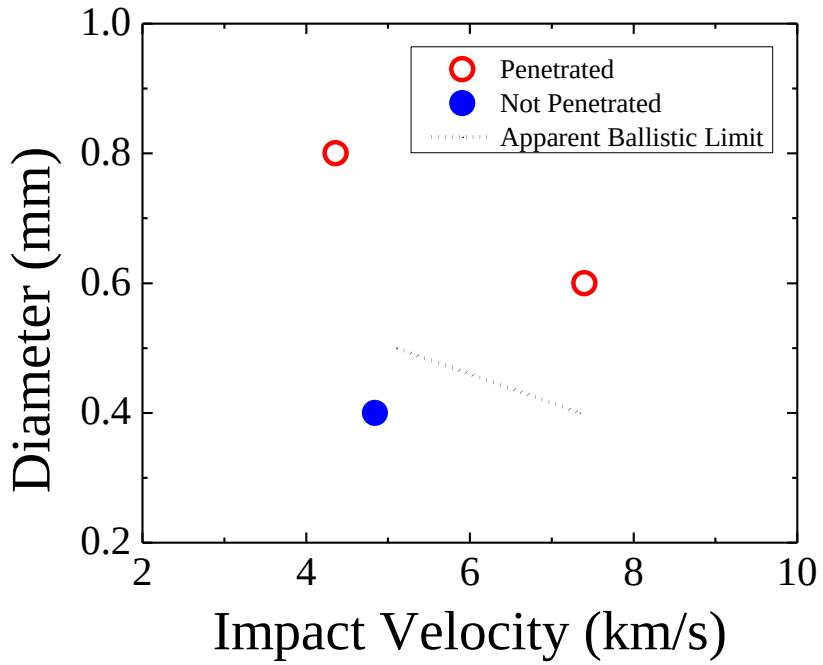

Fig. 7. Ballistic limit of prototype lay-ups containing STF-Armor™ plotted for projectile size as a function of impact velocity.

Table 1. Full hypervelocity impact testing matrix.

Diameter (mm)	Velocity (km/s)	Result	Thermal Energy to Vaporize (J)	Kinetic Energy at Impact (J)
0.4	4.84	Not Penetrated	1.3×10^{-6}	1.1
0.4	7.35	Apparent Ballistic Limit	1.3×10^{-6}	2.4
0.5	5.11	Apparent Ballistic Limit	2.6×10^{-6}	2.3
0.6	7.40	Penetrated	4.4×10^{-6}	8.4
0.8	4.36	Penetrated	1.1×10^{-5}	6.9

3.3 Hypervelocity Impact Damage Analysis

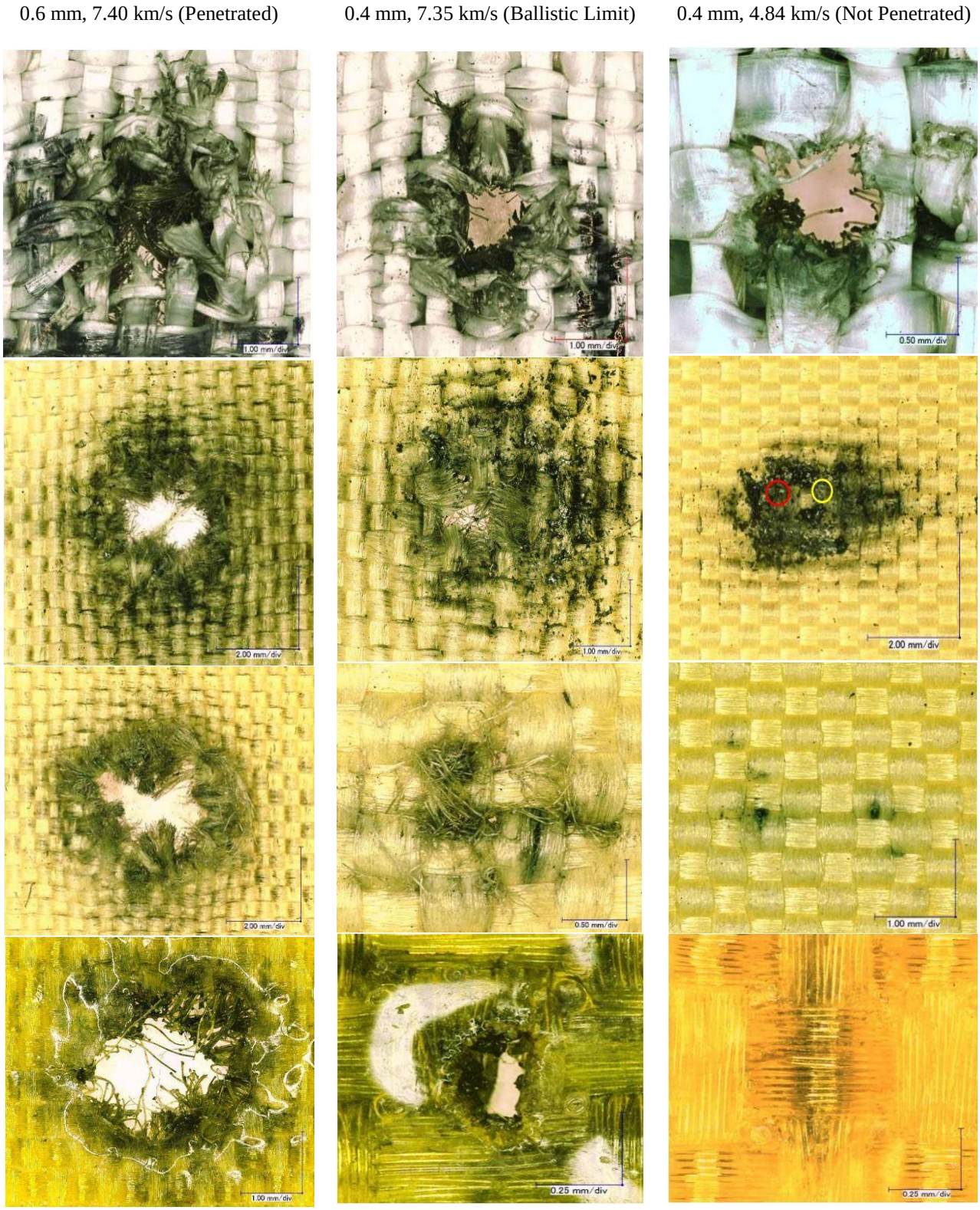

Fig 8. Damage to front of Orthofabric (top), front of 1st STF-Armor™ layer (second from top), rear of 2nd STF-Armor™ layer (second from bottom), and rear of urethane-coated nylon bladder cloth (bottom) for multiple projectile sizes and impact velocities.

Images of the damage zones to each layer in Figure 8 provide insight into the defeat mechanisms for each combination of projectile size and velocity. In all three cases, there was no debris or crater signature on the witness plates (not pictured). This would obviously be expected for the lay-up where the bladder cloth was not penetrated. For the targets that were penetrated and on the ballistic limit, this lack of a crater signature indicates that the projectiles were most likely completely vaporized upon impacting the Orthofabric. Indeed, simple thermodynamic calculations (Table 1) suggest that if a sizable fraction of the projectile's kinetic energy was converted to thermal energy upon impact, the aluminum projectile will vaporize.

A portion of the debris cloud was absorbed by the first STF-Armor™ layer in each case as evident by observing the small remnants of Mylar around the periphery of the damage zones. The first STF-Armor™ layer was penetrated in all tests, although the size of perforation is a strong function of the projectile's kinetic energy. A discernable difference in the defeat mechanism between the three cases is seen in the rear images of the second STF-Armor™ layer. In the cases of the lay-up completely penetrated (0.6 mm, 7.42 km/s), there is visual evidence of burn-through of the base Kevlar® textile. Conversion of the projectile's 8.4 J of kinetic energy into thermal energy upon impact likely resulted in temperatures exceeding the thermal degradation temperature of the Kevlar®. In contrast, thermal degradation of the Kevlar® was not an issue for lower energy impacts of a 0.4 mm projectile at 7.37 km/s and 0.4 mm at 4.85 km/s. In the former case, significant fibril breakage is observed, indicating that the maximum energy absorption capability of the STF-Armor™ was likely reached and thus, this projectile size and velocity combination is at the ballistic limit of the prototype lay-up. In the latter case, no significant fibril breakage is observed. Rather, small debris particles appear to have windowed between fibrils. Windowing is typically not an efficient projectile energy absorption mechanism so it is somewhat surprising that the bladder cloth remained completely intact. Given that the Kevlar® used was a correctional style with a tight weave and thinner yarns, the penetrating debris particles themselves were most likely sufficiently small such that they did not possess enough residual kinetic energy to puncture the bladder cloth. Finally, we can qualitatively compare these results to previous reports in literature and show that the lighter, thinner STF-Armor™ lay-ups investigated in this work show comparable performance to the standard EVA suit configuration [21].

4. Conclusion

The current work investigated the effects of replacing the existing neoprene-coated nylon absorber layer with STF-Armor™ on the MMOD and puncture resistance of the EVA suit. EVA suit lay-ups with STF-Armor™ as the absorber layers were significantly more effective against the cutting and puncture threats of hypodermic needles than those with neoprene-coated nylon under quasi-static loading conditions. A prototype EVA suit lay-up with STF-Armor™ was subjected to HVI testing and the ballistic limit identified. The results suggest that EVA suits containing STF-Armor™ can offer meaningful MMOD puncture protection while being lighter than the standard EVA suit. Further testing of the EVA suit lay-ups containing STF-Armor™ will be conducted on the International Space Station to evaluate the effect of the low-earth orbit environment on their stability and MMOD resistance. Analysis of the HVI results in the present work highlight areas where improvements can be made in successive generations of prototypes. Raising the ballistic limit will require addressing the thermal degradation experienced at higher projectile impact energies. Improvement strategies are being explored with regard to both the base textile substrate and the STF formulation as well.

Acknowledgements

The authors would like to acknowledge Alan Davis and Jon Read of the Hypervelocity Impact Testing Facility at Johnson Space Center as well as Don Henderson and the White Sands Remote Hypervelocity Test Facility team for assistance in the design of experiments and post-testing target analysis. This work was supported by a NASA EPSCoR Grant (NNX11AQ28A) and a Delaware Space Grant Graduate Fellowship (NNX10AN63H).

References

[1] Christiansen, E.L., Arnold, J., David, A., Hyde, J., Lear, D., Liou, J.-C., Lyons, F., Prior, T., Ratliff, M., Ryan, S., Giovane, F., Corsaro, B., and Studar, G., *Handbook for Designing MMOD Protection*, 2009, NASA.

[2] Whipple, F., 1947. Meteorites and Space Travels, Astronomical Journal 1161, p. 131.

[3] Jones, R., Graziosi, D., Ferl, J., Splawn, K., Zetune, D., Cadogen, D., and Christiansen, E.L., *Micrometeoroid and Orbital Debris Enhancements of Shuttle Extravehicular Mobility Unit Thermal Micrometeoroid Garment*, in *SAE Technical Paper*2006.
[4] Wagner, N.J. and Brady, J.F., 2009. Shear thickening in colloidal dispersions, Physics Today 62, p. 27-32.
[5] Mewis, J. and Wagner, N.J., 2012. Colloidal Suspension Rheology, Cambridge University Press, Cambridge.
[6] Cwalina, C.D. and Wagner, N.J., 2014. Material Properties of the Shear-Thickened State in Concentrated Near Hard-Sphere Colloidal Dispersions, Journal of Rheology 58, p. 949-967.
[7] Bender, J. and Wagner, N.J., 1996. Reversible shear thickening in monodisperse and bidisperse colloidal dispersions, Journal of Rheology 40, p. 899-916.
[8] Maranzano, B.J. and Wagner, N.J., 2001. The effects of interparticle interactions and particle size on reversible shear thickening: Hard-sphere colloidal dispersions, Journal of Rheology 45, p. 1205-12222.
[9] Maranzano, B.J. and Wagner, N.J., 2001. The effects of particle size on reversible shear thickening of concentrated colloidal dispersions, J Chem Phys 114, p. 10541-10527.
[10] Laun, H.M., Bung, R., and Schmidt, F., 1991. Rheology of Extremely Shear Thickening Polymer Dispersions (Passively Viscosity Switching Fluids), Journal of Rheology 35, p. 999-1034.
[11] O'Brien, V.T. and Mackay, M.E., 2000. Stress components and shear thickening of concentrated hard sphere suspensions, Langmuir 16, p. 7931-7938.
[12] Lee, Y.S., Wetzel, E.D., and Wagner, N.J., 2003. The ballistic impact characteristics of Kevlar (R) woven fabrics impregnated with a colloidal shear thickening fluid, Journal of Materials Science 38, p. 2825-2833.
[13] Decker, M.J., Halbach, C.J., Nam, C.H., Wagner, N.J., and Wetzel, E.D., 2007. Stab resistance of shear thickening fluid (STF)-treated fabrics, Composites Science and Technology 67, p. 565-578.
[14] Kalman, D.P., Merrill, R.L., Wagner, N.J., and Wetzel, E.D., 2009. Effect of Particle Hardness on the Penetration Behavior of Fabrics Intercalated with Dry Particles and Concentrated Particle-Fluid Suspensions, Acs Applied Materials & Interfaces 1, p. 2602-2612.
[15] Houghton, J.M., Schiffman, B.A., Kalman, D.P., Wetzel, E.D., and Wagner, N.J., 2007. "Hypodermic Needle Puncture of Shear Thickening Fluid (STF)-Treated Fabrics", SAMPE. pp. 1-11.
[16] Ryan, S., Christiansen, E.L., Davis, B.A., and Ordonez, E. Mitigation of EMU Cut Glove Hazard from Micrometeoroid and Orbital Debris Impacts on ISS Handrails, NASA TM-2009-0012274.
[17] Lee, S.-W.R. and Sun, C.T., 1993. A quasi-static penetration model for composite laminates, Journal of Composite Materials 27, p. 251-271.
[18] Lee, S.-W.R. and Sun, C.T., 1993. Dynamic Penetration of Graphite/Epoxy Laminates Impacted by a Blunt-Ended Projectile, Composites Science and Technology 49, p. 369-380.
[19] Jenq, S.T., Jing, H.-S., and Chang, C., 1994. Predicting the ballistic limit for plain woven glass/epoxy laminate, International Journal of Impact Engineering 15, p. 451-464.
[20] Sun, C.T. and Potti, S.V., 1996. A Simple Model to Predict Residual Velocities of Thick Composite Laminates Subjected to High Velocity Impacdt, International Journal of Impact Engineering 18, p. 339-353.
[21] Jones, R., Graziosi, D., Ferl, J., Splawn, K., Zetune, D., Cadogen, D., and Christiansen, E.L., *Micrometeoroid and Orbital Debris Enhancements of Shuttle Extravehicular Mobility Unit Thermal Micrometeoroid Garment*, in *SAE International*2006.

Appendix A. Projectile Velocity and Uncertainty

Projectile velocity is obtained with the following methods:

- Laser station consisting of two multi-beam lasers, LX1 and LX2.
- Muzzle laser is paired with either laser station or with photo diode to obtain velocity.
- Photo diode impact flash detectors are located at the stripper plate and target impact point

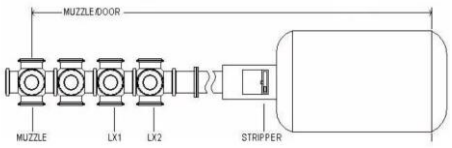

WSTF 17-Caliber Velocity Measurement Uncertainty Analyses Summary

.17-caliber Light Gas Gun

Measurement System	Laser LX1 to LX2	Muzzle Laser to LX1	Muzzle Laser to LX2	Muzzle Laser to Sabot Stripper	Muzzle Laser to Target
Random Uncertainty, ±	1.1%	0.5%	0.4%	0.8%	0.9%
Upper Bound Uncertainty, ±	1.8%	0.9%	0.6%	1.4%	1.2%

WSTF-IR-1086-001-07, April 16, 2007